Unraveling the Effect of Silanol Defects on the Insertion of Single-Site Mo in the MFI Zeolite Framework

Izabel Medeiros-Costa, Eddy Dib, Florent Dubray, Simona Moldovan, Jean-Pierre Gilson, Jean-Pierre Dath, Nikolai Nesterenko, Hristiyan Aleksandrov, Georgi Vayssilov, Svetlana Mintova

Unraveling the effect of silanol defects on the insertion of single site Mo in the MFI zeolite framework

Izabel C. Medeiros-Costa[a,b], Eddy Dib[a], Florent Dubray[a], Jean-Pierre Gilson[a], Jean-Pierre Dath[b], Nikolai Nesterenko[b], Hristiyan A. Aleksandrov[c], Georgi N. Vayssilov[c], and Svetlana Mintova[a,]*

[a] Normandie Université, Laboratoire Catalyse et Spectrochimie (LCS), ENSICAEN, UNICAEN, CNRS, 14050 Caen, France

[b] Total Research and Technology, Feluy, B-7181 Seneffe, Belgium

[c] Faculty of Chemistry and Pharmacy, University of Sofia, 1126 Sofia, Bulgaria

ABSTRACT. The preparation of defect-free MFI crystals containing single site framework Mo through a hydrothermal post-synthesis treatment is reported. The insertion of single Mo sites in the MFI zeolite samples with different crystal sizes of 100, 200 and 2000 nm presenting a diverse concentration of silanol groups is revealed. The nature of the silanols and their role in the incorporation of Mo into the zeolite structure are elucidated through an extensive spectroscopic characterization (^{29}Si NMR, ^{1}H NMR, ^{31}P NMR and IR) combined with X-ray diffraction and HRTEM. In addition, a DFT based theoretical modeling of a large $Si_{154}O_{354}H_{92}$ nanoparticle containing 600 atoms is carried out to understand the expansion of the unit cell volume measured by X-ray diffraction. An accurate quantification of the silanols in the MFI crystals with different particle sizes and the insertion of Mo in the zeolitic framework is reported for the first time. The results confirmed that the non H-bonded silanols seem to be the gateway for the insertion of single Mo atoms in the zeolite structure. Such materials with single metal sites present high crystallinity and perfect structure thus providing great stability in catalytic applications.

KEYWORDS. Defects, silanols, metals, zeolites, nanocrystals.

INTRODUCTION

Zeolites are microporous aluminosilicates with great applications in several areas as ion exchange, adsorption and catalysis.[1–3] The introduction of transition metals in zeolites e.g. Ti, Fe, V, Cu etc.[4–6] has been used as a way to enhance the zeolites performances and broaden their spectrum of use. The incorporation of metals can occur mainly in three different ways: ion exchange, impregnation of extra-framework metal oxides or isomorphic substitution.[7] The way

metals are incorporated into zeolites can change their properties considerably. Recently, it was shown that for the conversion of glycerol, Fe (III) in tetrahedral position was able to selectively generate acrylic acid, while, extra framework Fe (II) oxides selectively produced acrolein.[8] In the case of Mo-MFI catalysts used for methane conversion, the isomorphic substitution of Mo in a tetrahedral position appears as the most promising choice. In a previous publication of our group,[9] it was shown that the incorporation of single Mo atoms into the ZSM-5 framework was able to promote the activity, stability and reduce coke deposition when applied in methane conversion. On the other hand, the Mo impregnated ZSM-5 displayed fast deactivation because of the sintering and migration of molybdenum carbide species.[9] The Mo is inserted in the zeolite framework through a post-synthesis treatment.[10] A significant reduction in the silanol defects concentration in the zeolite is noticed after the incorporation of Mo, which is an evidence of their role in Mo insertion. Thus, in addition to creating new active sites, the introduction of Mo in the zeolitic structure favor the healing of silanol defects, commonly present in zeolites. Consequently, healing silanols with metals should also represent a step forward in applications where hydrophobic and/or highly stable zeolites are required. This approach might be useful for producing catalysts for applications such as non-oxidative methane conversion, hydrocracking and fluid catalytic cracking. The reduction of silanols content has also been shown to be important in several catalytic applications, where it is directly related to the reduction of coke deposition and to the increase of the catalyst lifetime.[11–14] Thus, the healing of silanol defects through the introduction of metals represents an attractive alternative to the classical method using hydrofluoric acid.[15]

Therefore, the relationship between the introduction of transition metals and silanol defects is highly important and needs to be investigated. In this contribution, we follow the post-synthesis

approach to insert Mo in pure silica MFI zeolites having different characteristics regarding the size of crystals and the amount and type of silanol defects. A full characterization of the zeolites before and after treatment with Mo permits to understand the mechanism of incorporation and distribution of Mo within the zeolite framework. The incorporation of Mo is more favorable in crystals presenting smaller size, which is likely related to the abundance of a specific type of silanols. Besides, a correlation was observed between the expansion of the unit cell volume and the amount of Mo incorporated, which agrees with the hypothesis of Mo isomorphic substitution. A, DFT based theoretical simulation indicates that Mo (VI) is the most stable oxidation state for this metal, when incorporated in the zeolite framework.

RESULTS AND DISCUSSION

Pure silica MFI zeolites were synthesized following the procedures described in the experimental section. The samples were named as MFI- x, where "x" represents the size of the zeolite crystals in nanometers. Samples MFI-100 MFI-200 and MFI-2000 contain zeolite crystals with particle size of 100, 200 and 2000 nm. The incorporation of Mo in these zeolite samples was carried out following the post-synthesis hydrothermal treatment procedure as described in our previous work.[10] Additional information is also provided in the method section. The nomenclature of zeolites after insertion of Mo was obtained by adding the prefix Mo- before the name of the parent zeolites (Mo-MFI-100, Mo-MFI-200 and Mo-MFI-2000). As shown in Figure 1, the zeolite crystals of sample Mo-MFI-100 have spherical morphology while the MFI-200 have more defined faces with hexagonal morphology. In turn, MFI-2000 presents twin zeolite crystals with the typical coffine-like shape morphology. The STEM-EDS elemental mapping shows a homogeneous distribution of Mo in the zeolite crystals with a mean Mo content of about 1.2, 1.0 and 0.16 wt. % for samples Mo-MFI-100, Mo-MFI-200 and Mo-MFI-2000, respectively.

Furthermore, the morphology and the size of the crystals was not affected by the hydrothermal post-synthesis treatment (Figure S1).

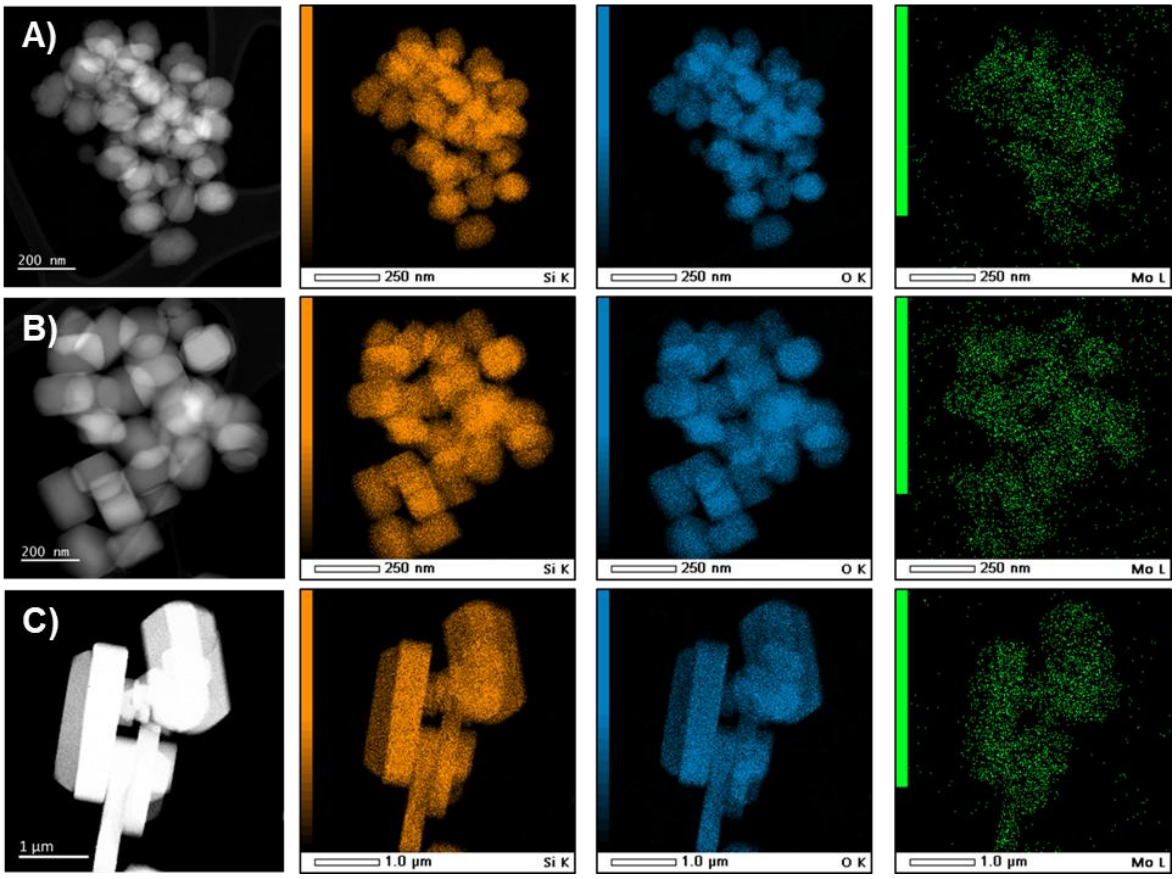

Figure 1. TEM micrographs and STEM-EDS elemental maps of samples (A) Mo-MFI-100, (B) Mo-MFI-200 and (C) Mo-MFI-2000 with the color code Si (orange), O (blue) and Mo (green).

Figure 2A shows the X-ray diffraction patterns of the zeolite samples before and after insertion of Mo. All zeolite samples present good crystallinity, which is maintained after the Mo incorporation. No Mo oxide phases were identified in the diffractograms, which is also supported by Raman analysis (Figure S2). The XRD patterns of the samples are presented in the range of

22.5° and 25 °2θ (Figure 2A); a splitting of the peaks at ~ 23.3°, 23.8° and 24.5° into two peaks marked with asterisks is observed for all Mo-containing samples, which evidences the monoclinic symmetry of the crystals. All as synthesized zeolite samples (MFI-100, -200 and -2000) before treatment with Mo, present orthorhombic symmetry, while after the incorporation of Mo (Mo-MFI-100, -200 and -2000) present monoclinic symmetry. The transition from orthorombic to monoclinic symmetry has already been observed after insertion of Al in the MFI zeolite framework.[16] The change in symmetry after the introduction of Mo in the zeolitic structure is accompanied by an increase in the unit cell volume. The unit cell volume of the as synthesized MFI-100, -200 and -2000 and Mo-containing Mo-MFI-100, -200 and -2000 zeolite samples obtained using Le Bail refinement considering the orthorombic and monoclinic symmetry, respectievely are shown in Figure 2B and Table S1. After the incorporation of Mo, the unit cell volume of all zeolite samples increases, even though the difference in the unit cell volume before and after incorporation of Mo is not the same for the different zeolites. A greater change in the unit cell volume for the samples with small zeolite crystal sizes (MFI-100 and MFI-200) is measured whereas that change is reduced in the case of big crystals (MFI-2000). The increase in unit cell volume of the Mo-MFI zeolites results from the incorporation of Mo in a tetrahedral position in the framework, since Mo (55 pm) has larger ionic radius than Si (40 pm). [17–19] Therefore, the more pronounced difference in unit cell volume in the case of smaller crystals is attributed to a greater incorporation of Mo atoms in the zeolitic framework. Therefore, small crystals can more easily receive a large amount of Mo in comparison to big crystals.

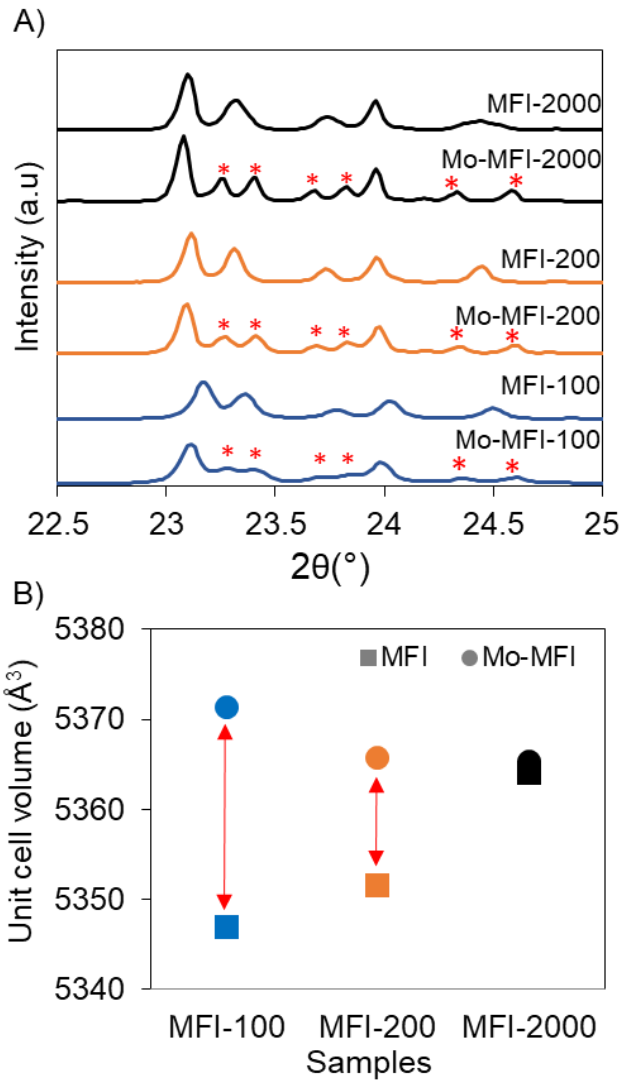

Figure 2. (A) X-ray diffraction patterns of samples MFI-100, MFI-200 and MFI-2000, Mo-MFI-100, Mo-MFI-100, Mo-MFI-200 and Mo-MFI-2000. (B) Unit cell volume calculated by means of Le Bail refinement of all samples. Samples are identified by the following color code: blue (MFI-100 and Mo-MFI-100), orange (MFI-200 and Mo-MFI-200) and black (MFI-2000 and Mo-MFI-2000); square symbols correspond to as-synthesized samples and circles correspond to Mo-containing samples.

The amount of Mo present in the zeolites was investigated through ^{31}P NMR, using trimethylphosphine oxide (TMPO) as a probe molecule. Two signals are clearly distinguished in the ^{31}P NMR spectra shown in Figure 3A, indicating different interactions of the TMPO molecule with the zeolite. The signal at 46 ppm corresponds to the interaction between the TMPO molecule and the Mo atom present in the zeolitic structure.[10] The signal at 30 ppm designates an excess of Free TMPO indicating that the quantity of TMPO used was sufficient to saturate all the Mo sites. Based on the area of the peak at 46 ppm and the amount of TMPO used, the amount of Mo incorporated in the zeolites is estimated, considering an equimolar ratio of TMPO and Mo.

The mass percentage of Mo per gram of zeolite for the different zeolite samples is shown in Figure 3B. The largest amounts of Mo (1.6 wt.%) is measured for the Mo-MFI-100 sample with the smallest zeolite crystals (100 nm). As the size of the zeolite crystals increases, a reduction in the quantity of incorporated Mo is measured. The amount of Mo in sample Mo-MFI-100 is slightly higher than in sample Mo-MFI-200 (1.3 wt.%). On the other hand, the zeolite with big crystals (sample Mo-MFI-2000) has only 0.4% wt. Mo. Although the results obtained from the quantification by EDS and ^{31}P NMR may differ slightly, the same trend is observed. The amount of Mo in the samples follows the order: Mo-MFI-100> Mo-MFI-200 >> Mo-MFI- 2000. As stated earlier, the insertion of Mo in the zeolite framework would be responsible for increasing the unit cell volume. In Figure 3C, the amount of Mo obtained through quantification by means of ^{31}P NMR is correlated to the difference in the unit cell volume measured for the samples before and after the introduction of Mo. A linear correlation is established between these parameters, which confirms the effect of the insertion of Mo in the change of the unit cell volume (Figure 3C).

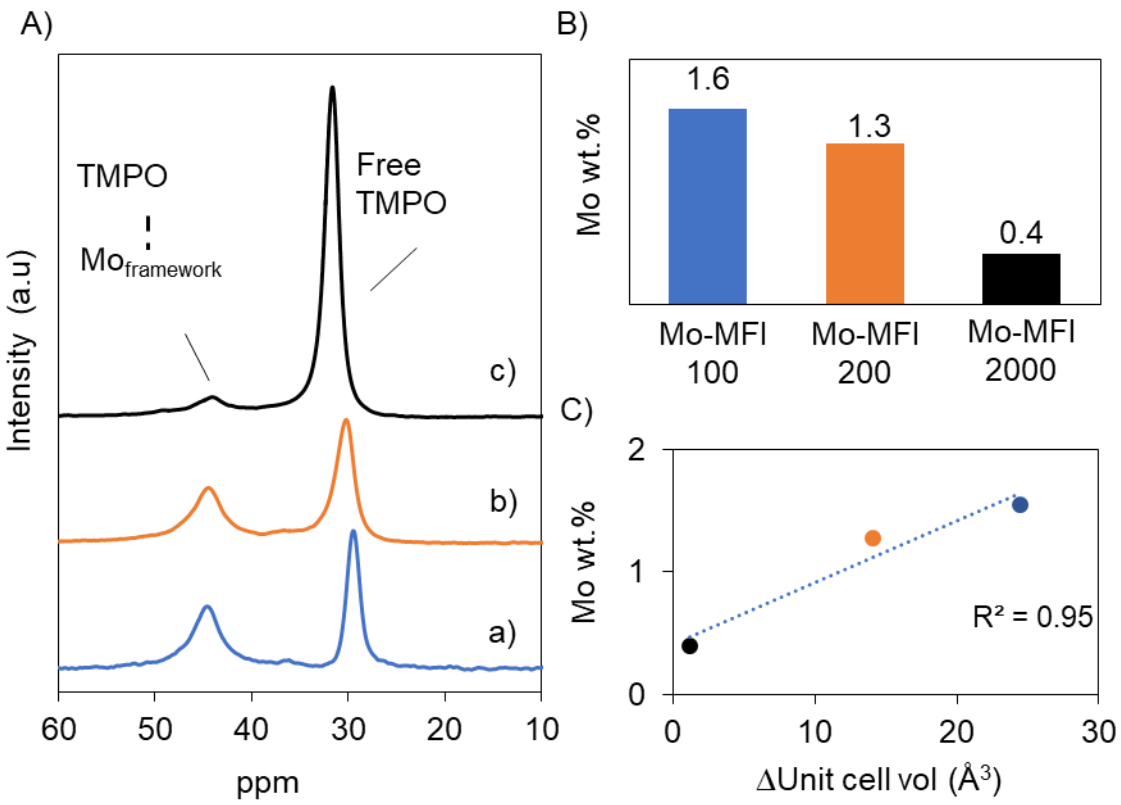

Figure 3. ^{31}P NMR spectra of samples Mo-MFI-100, Mo-MFI -200 and Mo-MFI -2000 (A). Mass percentage of Mo in the zeolites, calculated from the integration of the peak at 46 ppm in the ^{31}P NMR spectra (B). Correlation between the amount of Mo and the change in unit cell volume due to the introduction of Mo in the framework of the zeolites (C). Samples are identified by the following color code: (a) blue (Mo-MFI-100), (b) orange (Mo-MFI-200) and (c) black (Mo-MFI-2000).

Experimental studies have been supplemented by computational modeling based on periodic density functional calculations performed using the Vienna ab initio simulation package (VASP) [20,21] with the gradient corrected Perdew-Burke-Ernzerhof (PBE)[22] functional (see Experimental section for computational details). In order to clarify which is the most stable type of molybdenum ions in the zeolite framework we modeled three types of Mo-containing species

incorporated in the MFI framework (Figure 4 A-C). Similar to the situation with W-MFI zeolites[18] the most stable Mo-containing species incorporated in the MFI framework are Mo in oxidation state VI interacting with one additional O atom, MFI-[MoVIO]. When a H_2O molecule is dissociated at those MFI-[MoVIO] species and two hydroxyl groups are formed, the obtained MFI-[MoVI(OH)2] species is more stable by 11 kJ/mol than the MFI-[MoVIO], though one can expect that such a small energy difference can be easily overcome by the entropy contribution at room temperature and the water molecule is expected to desorb. The incorporation of MoIV species in oxidation state IV in the zeolite framework is considered as well. The obtained structure, MFI-[MoIV], is by 319 kJ/mol less stable than the most stable MFI-[MoVIO] structure; a similar results for W-containing MFI zeolites was also found where the MFI-[WVIO] is more stable than the MFI-[WIV] structure by >350 kJ/mol.[18]

In order to investigate the volume expansion of the MFI zeolite samples after Mo incorporation, we modeled a large $Si_{154}O_{354}H_{92}$ nanoparticle containing 600 atoms (Figure S3). It was a cut from the periodic MFI structure and the terminal oxygen centers were saturated by hydrogen, forming hydroxyl groups. The maximal distances between Si atoms at both ends of the nanoparticle at each direction (A, B, and C) are 17.23, 24.89, and 16.68 Å, respectively, thus the calculated volume of the nanoparticle is 7153.34 $Å^3$ (Table 1). To be more precise we averaged three equivalent Si-Si distances at each direction. Two or four silicon centers were substituted by [MoVIO] or by [$MoVI(OH)_2$] species, which corresponds to about 1.9 or 3.7 wt. % Mo in the zeolite nanoparticle, respectively. After incorporation of two and four [MoVIO]/[$MoVI(OH)_2$] species, the volume of the zeolite nanoparticles increases to 7234.78/7216.08 and 7325.05/7322.11 $Å^3$, respectively (Table 1). This increase corresponds to 0.9-1.1% and 2.3-2.4 % expansion of the unit cell volume of the zeolite nanoparticles containing two and four

molybdenum, respectively. These results are in a good agreement with experimental data (Figure 2).

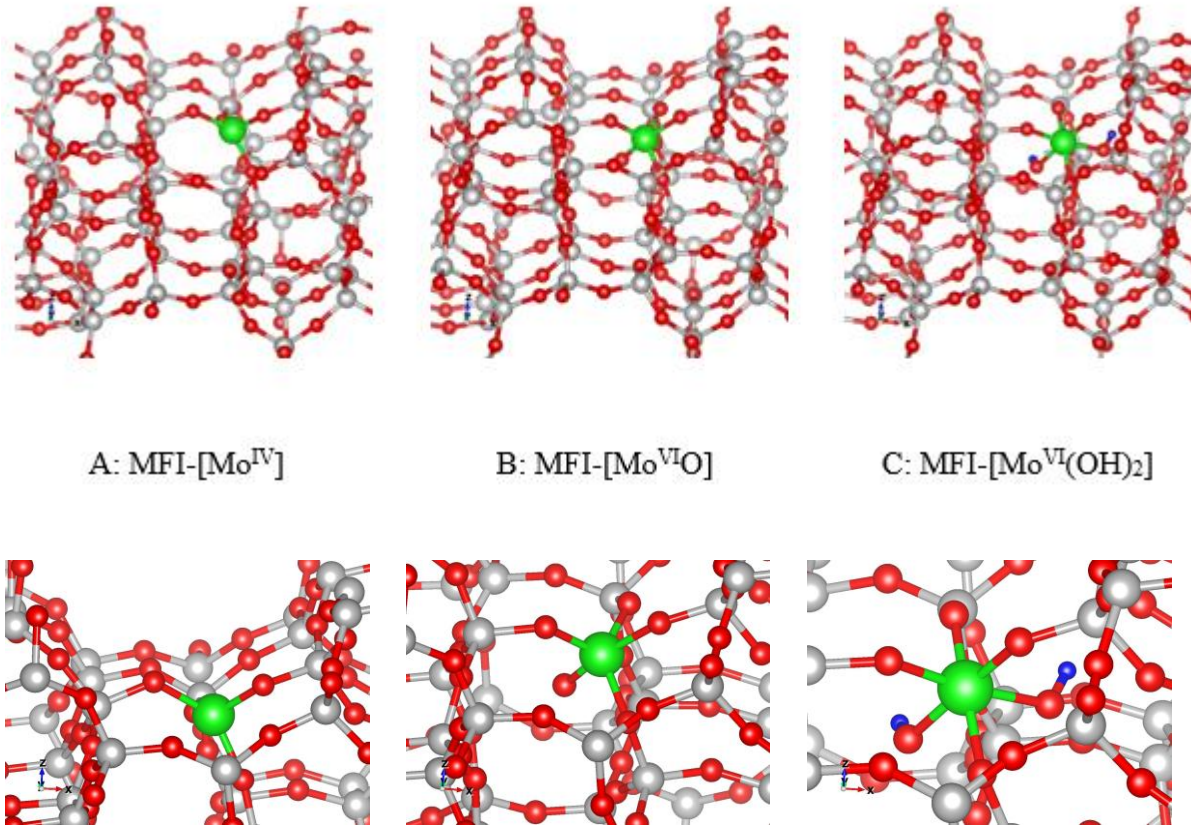

Figure 4. Optimized periodic bulk systems with Mo moieties incorporated in T11 position in the Mo-MFI zeolite structure. Color-coding: H (blue), O (red), Si (gray), and Mo (green).

Table 1. Si-Si distances (Å) between Si atoms located at the ends of the pristine pure silica zeolite nanoparticle as well as the nanoparticles containing two and four [MoVIO] or [MoVI(OH)$_2$] species incorporated in the pure silica zeolite nanoparticle. The unit cell volume (Å^3) of the pure silica and molybdenum containing zeolite nanoparticles and the volume expansion under incorporation of Mo in the structure are calculated.

	Direction A	Direction B	Direction C	Volume	Expansion, %
$Si_{154}O_{354}H_{92}$	17.23	24.89	16.68	7153.34	
$[MoO]_2Si_{152}O_{354}H_{92}$	17.22	24.99	16.81	7234.78	1.13
$[Mo(OH)_2]_2Si_{152}O_{354}H_{92}$	17.26	24.95	16.76	7216.08	0.87
$[MoO]_4Si_{150}O_{354}H_{92}$	17.27	25.04	16.93	7325.05	2.34
$[Mo(OH)_2]_4Si_{150}O_{354}H_{92}$	17.25	24.99	16.98	7322.11	2.30

So far, it is clear that the size of the crystals plays a role in the incorporation of Mo in the zeolitic framework. However, we have not yet addressed other features, as silanol defects, that also may affect the Mo incorporation. Just as the different zeolites presented throughout this work have different morphologies and crystal sizes, such zeolites also display different characteristics regarding the composition of silanol defects. Figures 5 and 6 show the IR and ^{1}H NMR spectra, respectively revealing different silanol groups of samples MFI-100, -200 and -2000 and Mo-MFI-100, -200 and -2000. Based on the positions of the bands in the IR spectra, the silanols are classified into two main groups, i.e., “non H-bonded silanols” and “H-bonded silanols” appearing in the range 3750-3650 cm-1 and 3500-3300 cm-1, respectively.[23]

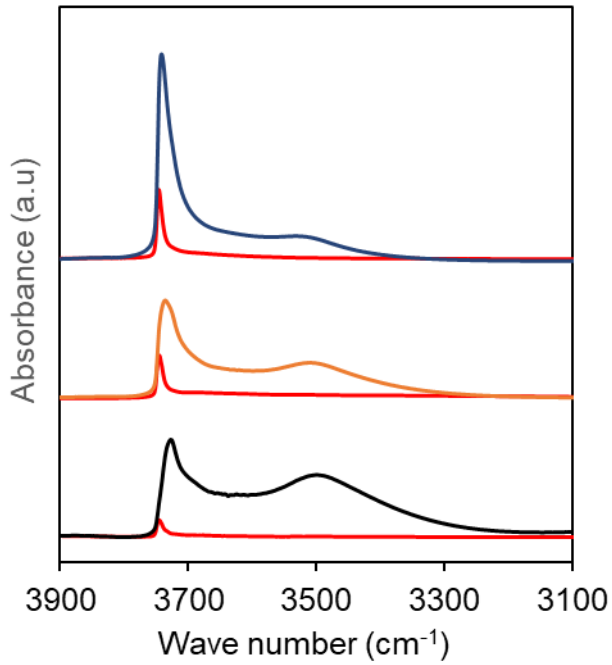

Figure 5. Characterization of silanol defects by IR spectroscopy: (a) MFI-100 (blue), (b) MFI-200 (orange) and (c) MFI-2000 (black) and samples Mo-MFI-100, Mo-MFI-200 and Mo-MFI-2000 are represented by a red solid line placed near the corresponding parent zeolite.

The ^{1}H NMR spectra are the mirror image of the IR spectra and also display non H-bonded silanols (~ 1-3ppm) and H-bonded silanols (~ 3-6 ppm), where according to the literature coincides with the zone for isolated/vicinal and H-bonded nest silanols, respectievely.[24] Non H-bonded silanol contributions increase in the zeolite samples with smaller crystal sizes. The ascending amount of non H-bonded silanols in the zeolite samples follow the order as MFI-2000 < MFI-200 < MFI-100. It is also noticed that the concentration of H-bonded silanols is lower for the small zeolite crystals (MFI-100) in comparison to the other two zeolite samples (MFI-200 and MFI-2000).

It is obvious from the ^{1}H NMR spectra that H-bonded silanols are completely healed by the introduction of Mo[10,25] Most of the non H-bonded silanols are also eliminated after the insertion

of Mo in the zeolite framework. As shown in Figure S4, a correlation can be drawn between the quantity of healed non H-bonded silanols and the quantity of Mo incorporated in the zeolite crystals, where samples with higher amount of non H-bonded silanols also present higher amount of Mo after the hydrothermal post-treatment (Mo-MFI-100>Mo-MFI-200>Mo-MFI-2000). On the other hand, no trend is observed when correlating H-bonded silanols and the quantity of Mo in the samples. For this reason, we believe that Mo atoms are preferentially bonded to non H-bonded silanols, which present convenient configuration with free space to receive Mo atoms.

In order to provide more insights into the relationship between the healing of silanols and Mo insertion in the zeolitic structure, ^{1}H NMR (silanols) and ^{31}P NMR (Mo) quantitative data are presented in Figure 7. To enable the comparison between the amount of healed silanols and the amount of Mo introduced into the zeolite framework, both molar amounts of H-bonded and non H-bonded silanols were divided by four, respecting the 4 SiOH: 1 Mo stoichiometry. This stoichiometry was deduced from theoretical calculations, which indicate that the most stable configuration for the Mo atom is found when it is linked to the zeolitic structure through four bonds. Thus, an excess of healed silanols is measured relatively to the amount of Mo inserted into the zeolite samples (Mo-MFI-100, -200 and -2000) (Figure 7). Excess silanols are observed regardless the type of silanol: H-bonded or non H-bonded silanols. An extreme case for the Mo-MFI-2000 sample, where the crystals have large amounts of H-bonded healed silanols, although it presents a small incorporation of Mo is found. These information led us to conclude that Mo is not the only agent responsible for the defects healing. A partial recrystallization of the zeolite structure during the post synthesis hydrothermal treatment is possibly occurred leading to defects healing.

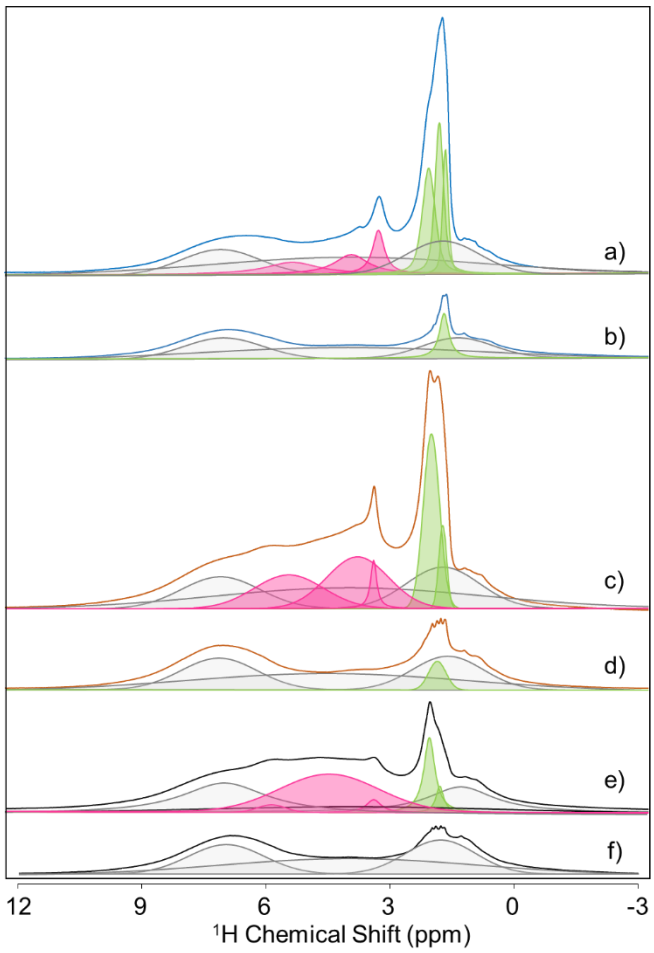

Figure 6. ^{1}H NMR spectra of samples (a) MFI-100, (b) Mo-MFI-100, (c) MFI-200, (d) Mo-MFI-200 and (e) MFI-2000 and (f) Mo-MFI-2000. The deconvolution of the signals includes: non-H-bonded silanols (green), H-bonded silanols (pink) and the signal from the rotor (gray).

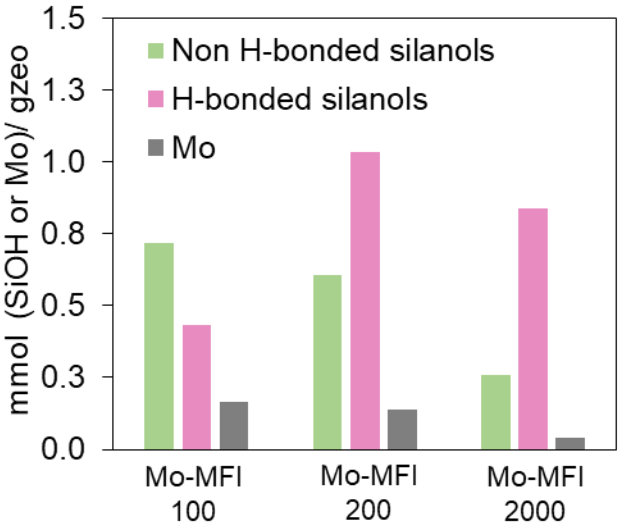

Figure 7. Comparison between the quantities of Mo (gray bars) and different types of silanols healed during the post-synthesis insertion of Mo in the zeolite samples. The quantities of healed silanols were calculated from the difference of silanols in the parent zeolite samples (MFI-100, -200 and -2000) and remaining silanols after Mo insertion (Mo-MFI-100, -200 and 2000). Both H-bonded (pink bars) and non H-bonded silanols (green bars) are presented. Mols of silanols (green and pink bars) were divided by four in order to respect the stoichiometry where one Mo atom bonds with four oxygens of the zeolite (oxygens from silanol groups in the parent MFI zeolites).

The healing of defects through the hydrothermal post-synthesis treatment with Mo is further confirmed by means of ^{29}Si NMR spectroscopy. ^{29}Si NMR spectra are shown in Figure 8, parent MFI-100, MFI-200 and MFI-2000 zeolite samples present a Q^3 signal, indicating the presence of silanol defects. In addition, a low-resolution Q^4 signal in all spectra is observed, which is also typical of the presence of defects in the framework structure. After hydrothermal post-synthesis treatment with Mo, Q^3silanol signals are no longer present in samples Mo-MFI-100, -200 and -

2000 and a remarkable increase in the homogeneity of the structures is evidenced through the high resolution of the Q^4 signal.[10,26] Through ^{29}Si NMR we can also confirm the hypothesis raised previously about the fact that Mo is not the single responsible for healing silanols, since the Mo-MFI-2000 sample displays a highly resolved Q^4 signal, even though it has low Mo incorporation.

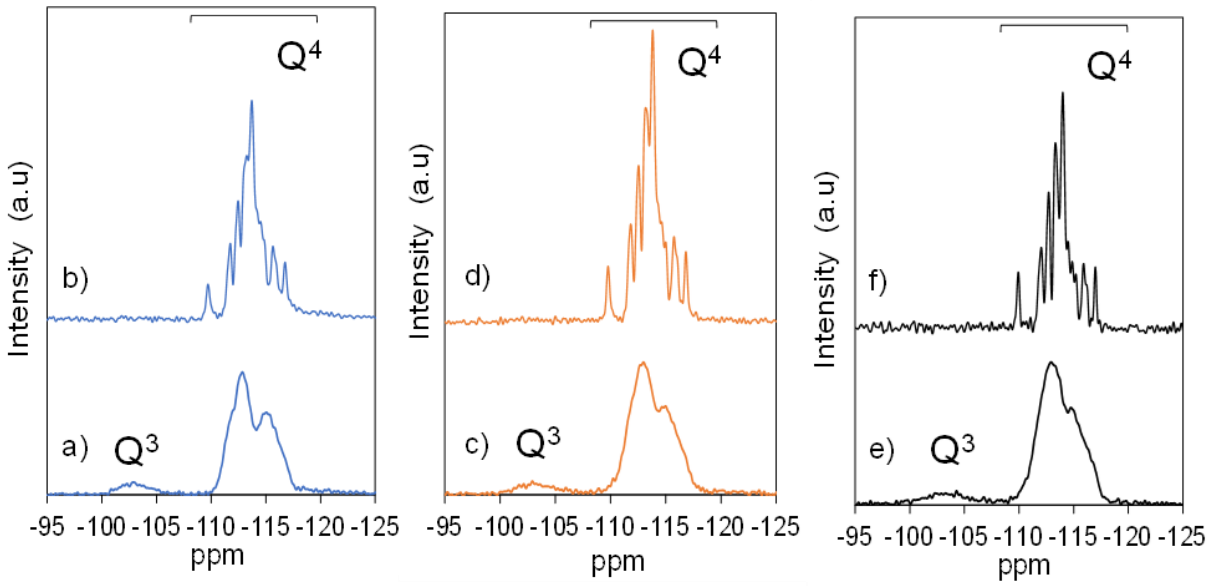

Figure 8. ^{29}Si NMR spectra of samples (a) MFI-100, (b) Mo-MFI-100, (c) MFI-200, (d) Mo-MFI-200, (e) MFI-2000 and (f) Mo-MFI-2000.

CONCLUSION

Mo-MFI zeolites with different crystal sizes (100 nm, 200 nm and 2000 nm) are prepared by hydrothermal post-synthesis treatment of pure silica MFI zeolites. The Mo-MFI zeolites present perfect crystals with no significant amounts of silanol defects, as observed by ^{29}Si NMR, ^{1}H NMR and IR. The successful incorporation of Mo in the zeolite framework and its homogeneous

distribution is directly accessed through ^{31}P NMR and STEM-EDS. Furthermore, the insertion of Mo into the zeolitic structure generates an orthorhombic-monoclinic phase transition, which is accompanied by an increase in the unit cell volume. The expansion of the unit cell by the insertion of Mo is also confirmed by the DFT calculations. The results indicate that the MFI-[MoVIO] is the most stable configuration for the insertion of Mo in the MFI framework structure. The incorporation of the Mo is favored in the case of zeolite nanocrystals (100 nm and 200 nm) relatively to the micron-sized crystals (2000 nm). Moreover, Mo atoms are likely to connect to non H-bonded silanols, more abundant in the nanocrystals in comparison to micron-sized zeolite. The healing of H-bonded silanols is also achieved by the hydrothermal treatment, however it should not be directly linked to the incorporation of Mo. This approach presents a high potential for introduction of single site metal species in zeolite crystals containing various defect sites. The single site metal catalysts are of great importance sine high stability of the catalysts working outside of the comfort zone is required.

METHODS

Synthesis of parent MFI zeolites. As shown in Table 2, the MFI zeolites were prepared from precursor suspensions with various molar compositions. Double distilled water and TPAOH (tetra n-propylammonium hydroxide, 20 wt% in water solution, Alfa Aesar) were initially mixed for about 30 minutes, followed by dropwise addition of TEOS (tetraethyl orthosilicate, 98%, Aldrich). The precursor solutions were kept under magnetic stirring for 1 h after adding TEOS, then aged for 18 hours at room temperature on an orbital shaker. The hydrothermal treatment of the aged suspensions was carried out in polypropylene bottles at 90 °C or in Teflon lined stainless steel autoclaves at 140 °C. In both cases, the syntheses were performed under autogenous pressure and static conditions. After the crystallization period (detailed for each

sample in Table 2), the samples were purified, dried overnight at 90 ° C and calcined at 550 ° C/ 5h.

Table 2. Molar composition of the precursor suspensions used for the synthesis of zeolites and the respective hydrothermal (HT) conditions

MFI-100	
Molar composition	$1SiO_2$:0.28 TPAOH: 40 H_2O
HT conditions	48 h/ 90 °C
MFI-200	
Molar composition	$1SiO_2$:0.28 TPAOH: 40 H_2O
HT conditions	6 h/ 180 °C
MFI-2000	
Molar composition	$1SiO_2$:0.14 TPAOH: 40 H_2O
HT conditions	15 days/ 140 °C

Incorporation of Mo in MFI zeolites. The calcined zeolites were treated with a 3% wt. solution of $Na_2MoO_4.2H_2O$ in a ratio of 21.5 g of solution per 1 gram of zeolite samples. The mixtures of zeolite and sodium molybdate solution were placed in closed polypropylene bottles and stirred for one hour at room temperature. The bottles were then placed in the oven at 90 °C under static conditions for a period of 7 days. After hydrothermal treatment, the zeolites were washed extensively with double deionized water. The solids recovered by centrifugation were dried overnight at 90 ° C and calcined at 550 °C/ 5h. After calcination, the samples were ion exchanged with 0.2 M NH_4Cl solution. Two cycles of ion exchange were performed and in each cycle the mixture was stirred for one hour at room temperature and the zeolites recovered by

centrifugation. At the end of the second cycle, the solids were rinsed with double distilled water, recovered again by centrifugation and placed in the oven at 90 °C, where they were dried overnight and then calcined at 550 ° C / 5h. After treatment with Mo and subsequent ion exchange, the samples were named by adding Mo to the respective names of the parent zeolites: Mo-MFI-100, Mo-MFI-200 and Mo-MFI-2000.

X-Ray Diffraction (XRD). X-Ray diffraction patterns were acquired using a PANanalytical X'Pert Pro diffractometer equipped with a Johansson monochromator, Kα1 radiation λ = 1.540598 Å. The patterns were measured with a step of 0.0167 °. JANA2006 software was used to perform Le Bail profile refinement and thus determine unit cell parameters (Table S1).[27]

Transmission Electron Microscopy (TEM). The crystal size and morphology were measured by transmission electron microscopy (TEM); experiments were carried out on an Analythical double (objective and probe) corrected JEOL ARM200CF equipped with a 100 mm Centurio EDS detector and a Quantum GIF for the EELS. A probe of 0.1 nm was used to scan the specimen in STEM mode and Bright Field, and high Angular Annular Dark Field detectors were simultaneously employed for imaging. The camera length was fixed at 8 cm. To avoid material degradation, the STEM-EDS analytical essays were carried out at 80 kV with a high scanning speed of 3 µs/px and for a mean duration of 60 minutes.

Fourier Transform Infrared Spectroscopy (FTIR). FTIR spectra were obtained by using a Nicolet Magna 550-FT-IR spectrometer (4 cm-1 optical resolution). Zeolite wafers with an average area of 1cm2 and about 20 mg were hydraulic pressed (1.5 t.cm-²). The self-supported wafers were activated at 500 °C for 4 hours under secondary vacuum prior to the measurements.

Nuclear Magnetic Resonance Spectroscopy (NMR). ^{1}H, ^{29}Si and ^{31}P NMR analyzes were performed on a 11.7 T Bruker Avance 500 spectrometer operating at a frequency of 500.07 MHz, 99.35 MHz and 202.4 MHz, respectively. In the case of ^{31}P and ^{29}Si NMR, the samples were packed into 3.2 mm zirconia rotors that spun at 22 kHz. In order to obtain higher resolution in the case of ^{1}H NMR, 1.9 mm zirconium rotor was used at a spinning rate of 40 kHz. Flip angles of 30° was used when measuring ^{29}Si NMR spectra, while 90° flip angles were used for ^{1}H and ^{31}P NMR spectra. The number of scans of single-pulse ^{1}H, ^{29}Si and ^{31}P MAS NMR was 64, 2048 and 256, respectively. Tetramethyl silane (TMS) was used as a reference for the chemical shift of ^{1}H and ^{29}Si NMR and phosphoric acid (H_3PO_4) for ^{31}P NMR experiments.

Sample preparation for ^{31}P NMR: The presence of Mo atoms in the zeolitic structure was investigated through ^{31}P NMR by using trimethylphosphine oxide (TMPO) as a probe molecule. The samples were initially activated under secondary vacuum at 400 °C for 5 h. Then, the cell containing the sample was sealed and placed in a glovebox under Ar. The TMPO was weighed inside the glovebox, dissolved with dichloromethane and the solution was transferred to the cell containing the sample with the aid of a syringe. The volume of TMPO/ dichloromethane solution was about 0.8 ml and it was sufficient to immerse the zeolite powder. The cell was then placed in the ultrasound bath for 15 min and the zeolite/TMPO- dichloromethane mixture was kept inside the cell overnight. The next day the dichloromethane was evaporated in a rotavapor and the cell was again placed under secondary vacuum in order to remove any traces of the solvent. As a result, the solid zeolite + adsorbed TMPO was obtained and used to fill the 3.2 mm zirconium NMR rotor (under Ar atmosphere). Sample preparation for ^{1}H NMR: Before measurements samples were activated at 350 ° C/10 h under secondary vacuum. The 1.9 mm zirconium rotor filled with the dehydrated zeolite were closed under Ar atmosphere.

Computational Modeling. The periodic plane wave quantum chemical calculations performed with the Vienna ab initio simulation package (VASP)[20,21]were based on the density functional theory method using a cutoff energy of 415 eV. The gradient corrected Perdew-Burke-Ernzerhof (PBE),[22] exchange-correlation functional with the additional empirical dispersion correction (PBE+D2)[28] and PAW pseudopotentials were employed.[29,30] For the bulk calculations an orthorhombic unit cell of the MFI type zeolite framework, consisting of 96 T atoms with dimensions a = 20.271 Å, b = 19.925 Å, c = 13.332 Å was used,[31] while the $Si_{154}O_{354}H_{92}$ nanoparticle were model in an orthorhombic unit cell with dimensions: a = 27.271 Å, b = 26.925 Å, c = 33.664 Å. Due to the large size of the unit cells, the Brillouin zone using only the Γ point was samples.[32]All atoms of zeolite structures were allowed to relax until the force on each atom becomes less than 5×10^{-4} eV/pm during the geometry optimization.

Corresponding Author

*svetlana.mintova@ensicaen.fr

Author Contributions

The manuscript was written through contributions of all authors. All authors have given approval to the final version of the manuscript.

ACKNOWLEDGMENT

This research was supported by TOTAL and Industrial Chair ANR-TOTAL “Nanoclean energy”, the Normandy University, and the Lable of Excellence for the Centre of Zeolites and Nanoporous Materials by the Region of Normandy. H. A. A. and G. N. V. acknowledge support

by the European Regional Development Fund and the Operational Program “Science and Education for Smart Growth” under contract UNITe No. BG05M2OP001-1.001-0004-C01.

Supporting Information

A supporting information file is available presenting SEM and Raman analyses, as well as correlations between ^{1}H NMR data and Mo quantification. Additional details on LeBail calculation and molecular modeling are also presented.

REFERENCES

(1) Dusselier, M.; Davis, M. E. Small-Pore Zeolites: Synthesis and Catalysis. *Chem. Rev.* **2018**, *118* (11), 5265–5329. https://doi.org/10.1021/acs.chemrev.7b00738.

(2) Weckhuysen, B. M.; Yu, J. Recent Advances in Zeolite Chemistry and Catalysis. *Chem. Soc. Rev.* **2015**, *44* (20), 7022–7024. https://doi.org/10.1039/c5cs90100f.

(3) Kulprathipanja, S.; James, R. B. Overview in Zeolites Adsorptive Separation. In *Zeolites in industrial separation and Catalysis*; Kulprathipanja, S., Ed.; Wiley- VCH Verlag GmbH & Co. KGaA, 2010; pp 173–201. https://doi.org/10.1002/9783527629565.

(4) Taramasso, M.; Milanese, S.; Perego, G.; Milan; Notari, B. Preparation of Porous Crystalline Synthetic Material Comprised of Silicon and Titanium Oxides. US4410501A, 1983.

(5) Millini, R.; Perego, G.; Bellussi, G. Synthesis and Characterization of Boron- containing Molecular Sieves. *Top. Catal.* **1999**, *9* (1), 13. https://doi.org/10.1023/A:1019198119365.

(6) Dzwigaj, S.; Massiani, P.; Davidson, A.; Che, M. Role of Silanol Groups in the Incorporation of V in β Zeolite. *J. Mol. Catal. A Chem.* **2000**, *155* (1–2), 169–182. https://doi.org/10.1016/S1381-1169(99)00332-5.

(7) Clatworthy, E. B.; Konnov, S. V; Dubray, F.; Nesterenko, N.; Gilson, J.; Mintova, S. Emphasis on the Properties of Metal-Containing Zeolites Operating Outside the Comfort Zone of Current Heterogeneous Catalytic Reactions Angewandte. *Angew. Chem. Int. Ed.* **2020**, *59*, 19414–19432. https://doi.org/10.1002/anie.202005498.

(8) Diallo, M. M.; Laforge, S.; Pouilloux, Y.; Mijoin, J. Influence of the Preparation Procedure and Crystallite Size of Fe-MFI Zeolites in the Oxidehydration of Glycerol to Acrolein and Acrylic Acid. *Catal. Commun.* **2019**, *126* (January), 21–25. https://doi.org/10.1016/j.catcom.2019.04.014.

(9) Konnov, S. V.; Dubray, F.; Clatworthy, E. B.; Kouvatas, C.; Gilson, J.; Dath, J.; Minoux, D.; Aquino, C.; Valtchev, V.; Moldovan, S.; Koneti, S.; Nesterenko, N.; Mintova, S. Novel Strategy for the Synthesis of Ultra- Stable Single- Site Mo- ZSM- 5 Zeolite Nanocrystals. *Angew. Chemie* **2020**, No. 59, 19553– 19560. https://doi.org/10.1002/ange.202006524.

(10) Dubray, F.; Moldovan, S.; Kouvatas, C.; Grand, J.; Aquino, C.; Barrier, N.; Gilson, J.; Nesterenko, N.; Minoux, D.; Mintova, S. Direct Evidence for Single Molybdenum Atoms Incorporated in the Framework of MFI Zeolite Nanocrystals. *J. Am. Chem. Soc.* **2019**, *141*, 8689–8693. https://doi.org/10.1021/jacs.9b02589.

(11) Lee, K.; Lee, S.; Jun, Y.; Choi, M. Cooperative Effects of Zeolite Mesoporosity and Defect Sites on the Amount and Location of Coke Formation and Its Consequence in Deactivation. *J. Catal.* **2017**, *347*, 222–230. https://doi.org/10.1016/j.jcat.2017.01.018.

(12) Prokopyeva, I.; Goetze, J.; Gucuyener, C.; Van Thiel, L.; Dikhtiarenko, A.; Ruiz-Martinez, J.; Weckhuysen, B.; Gascon, J.; Kapteijn, F. Methanol-to-Olefins Process over Zeolite Catalysts with DDR Topology: Effect of Composition and Structural Defects on Catalytic Performance. *Catal. Sci. Technol.* **2016**, *6*, 2663–2678. https://doi.org/10.1039/C5CY02140E.

(13) Grahn, M.; Faisal, A.; Öhrman, O. G. W.; Zhou, M.; Signorile, M.; Crocellà, V.; Sadegh, M.; Hedlund, J. Small ZSM-5 Crystals with Low Defect Density as an Effective Catalyst for Conversion of Methanol to Hydrocarbons. *Catal. Today* **2020**, *345*, 136–146. https://doi.org/10.1016/j.cattod.2019.09.023.

(14) Qin, Z.; Lakiss, L.; Tosheva, L.; Gilson, J. Comparative Study of Nano-ZSM-5 Catalysts Synthesized in OH - and F - Medium. *Adv. Funct. Mater.* **2014**, *24* (2), 257–264. https://doi.org/DOI: 10.1002/adfm.201301541.

(15) Axon, S. A.; Klinowski, J. Synthesis and Characterization of Defect-Free Crystals of MFI-Type Zeolites. *Appl. Catal. A Gen.* **1992**, *81* (1), 27–34. https://doi.org/doi.org/10.1016/0926-860X(92)80258-E.

(16) van Koningsveld, H.; Tuinstra, F.; Jansen, J. C.; van Bekkum, H. On the Preparation of a Monoclinic (Nearly) Single Crystal of Zeolite HZSM-5. *Zeolites* **1989**, *9* (3), 253–256. https://doi.org/10.1016/0144-2449(89)90035-3.

(17) Deka, R. C.; Nasluzov, V. A.; Ivanova Shor, E. A.; Shor, A. M.; Vayssilov, G. N.; Rösch, N. Comparison of All Sites for Ti Substitution in Zeolite TS-1 by an Accurate Embedded-Cluster Method. *J. Phys. Chem. B* **2005**, *109* (51), 24304–24310. https://doi.org/10.1021/jp050056l.

(18) Borin, M. F.; Silva, T. Da; Felisbino, R. F.; Cardoso, D. Synthesis of TS-1 Molecular Sieves Using a New Ti Source. *J. Phys. Chem. B* **2006**, *110* (31), 15080–15084. https://doi.org/10.1021/jp060703o.

(19) Tuel, A.; Taârit, Y. Ben. Influence of the Nature of Silicon and Titanium Alkoxides on the Incorporation of Titanium in TS-1. *Appl. Catal. A, Gen.* **1994**, *110* (1), 137–151. https://doi.org/10.1016/0926-860X(94)80112-6.

(20) Kresse, G.; Furthmüller, J. Efficiency of Ab-Initio Total Energy Calculations for Metals and Semiconductors Using a Plane-Wave Basis Set. *Comput. Mater. Sci.* **1996**, *6* (1), 15–50. https://doi.org/10.1016/0927-0256(96)00008-0.

(21) Kresse, G.; Hafner, J. *Ab Initio* Molecular-Dynamics Simulation of the Liquid-Metal–Amorphous-Semiconductor Transition in Germanium. *Phys. Rev. B* **1994**, *49* (20), 14251–14269. https://doi.org/10.1103/PhysRevB.49.14251.

(22) Perdew, J. P.; Burke, K.; Ernzerhof, M. Generalized Gradient Approximation Made Simple. *Phys. Rev. Lett.* **1996**, *77* (18), 3865–3868. https://doi.org/10.1103/PhysRevLett.77.3865.

(23) Bordiga, S.; Ugliengo, P.; Damin, A.; Lamberti, C.; Spoto, G.; Zecchina, A.; Spanò, G.; Buzzoni, R.; Dalloro, L. Hydroxyls Nests in Defective Silicalites and Strained Structures Derived upon Dehydroxylation : Vibrational Properties and Theoretical Modelling. *Top. Catal.* **2001**, *15* (1), 43–52. https://doi.org/10.1023/A:1009019829376.

(24) Arzumanov, S. S.; Stepanov, A. G. Which Activation Energy Do We Measure? Analysis of the Kinetics of Propene-3-13C Double-Bond-Shift Reaction on Silicalite-1 by 1H MAS NMR

in Situ. *J. Phys. Chem. C* **2018**, *122* (41), 23432–23440. https://doi.org/10.1021/acs.jpcc.8b06044.

(25) Grand, J.; Talapaneni, S. N.; Vicente, A.; Fernandez, C.; Dib, E.; Aleksandrov, H. A.; Vayssilov, G. N.; Retoux, R.; Boullay, P.; Gilson, J.; Valtchev, V.; Mintova, S. One-Pot Synthesis of Silanol-Free Nanosized MFI Zeolite. *Nature* **2017**, *16* (July), 1010–1015. https://doi.org/10.1038/NMAT4941.

(26) Chezeau, J. M.; Delmotte, L.; Guth, J. L.; Gabelica, Z. Influence of Synthesis Conditions and Postsynthesis Treatments on the Nature and Quantity of Structural Defects in Highly Siliceous MFI Zeolites: A High-Resolution Solid-State 29Si n.m.r. Study. *Zeolites* **1991**, *11* (6), 598–606. https://doi.org/10.1016/S0144-2449(05)80011-9.

(27) Petříček, V.; Dušek, M.; Palatinus, L. Crystallographic Computing System JANA2006: General Features. *Z. Krist.* **2014**, *229* (5), 345–352.

(28) Grimme, S. Semiempirical GGA-Type Density Functional Constructed with a Long-Range Dispersion Correction. *J. Comput. Chem.* **2006**, *27* (15), 1787–1799. https://doi.org/https://doi.org/10.1002/jcc.20495.

(29) Blöchl, P. E. Projector Augmented-Wave Method. *Phys. Rev. B* **1994**, *50* (24), 17953–17979. https://doi.org/10.1103/PhysRevB.50.17953.

(30) Kresse, G.; Joubert, D. From Ultrasoft Pseudopotentials to the Projector Augmented-Wave Method. *Phys. Rev. B* **1999**, *59* (3), 1758–1775. https://doi.org/10.1103/PhysRevB.59.1758.

(31) Baerlocher, C.; L. B. McCusker. Database of Zeolite Structures. http://www.iza-structure.org/databases http://www.iza-structure.org/databases.

(32) Jeanvoine, Y.; G. Ángyán, J.; Kresse, G.; Hafner, J. Brønsted Acid Sites in HSAPO-34 and Chabazite: An Ab Initio Structural Study. *J. Phys. Chem. B* **1998**, *102* (29), 5573–5580. https://doi.org/10.1021/jp980341n.